Hindawi
Mathematical Problems in Engineering
Volume 2018, Article ID 8402601, 9 pages
https://doi.org/10.1155/2018/8402601

Research Article

Mobilizable Strength Design for Multibench Retained Excavation

Gang Zheng,[1,2] Fanjun Wang,[2] Dong-qing Nie,[3] Yu Diao ,[1,2] Danyao Yu,[2] and Xuesong Cheng [1,2]

[1] *MOE Key Laboratory of Coast Civil Structure Safety, Tianjin University, 92 Weijin Rd., Nankai District, Tianjin 300072, China*
[2] *Department of Civil Engineering, Tianjin University, 92 Weijin Rd., Nankai District, Tianjin 300072, China*
[3] *Design Institute 4, Shanghai Municipal Engineering Design Institute (Group) Co., Ltd., 901 Zhongshan Rd. (North 2), Yangpu District, Shanghai 200092, China*

Correspondence should be addressed to Xuesong Cheng; cheng_xuesong@163.com

Received 7 February 2018; Accepted 8 April 2018; Published 13 May 2018

Academic Editor: Manuel Pastor

Multibench retaining systems can be used in large area excavations for the purpose of eliminating horizontal struts. However, there is no design method for this retaining system. Based on the mobilizable strength design (MSD) concept, a design procedure for a two-bench retaining system considering the interaction of the first and second retaining structures was proposed and tested. Based on an admissible strain field for a two-bench retained excavation in undrained condition, the shear strain in the superimposed strain and the lateral earth pressure distribution acting on the retaining structures can be determined. Then, the mobilized shear strength corresponding to the strain field could be calculated by the equations of force and moment equilibrium. Further, the crest displacements, earth pressures, and bending moment in a two-bench retained excavation can be calculated. The calculated results using MSD were verified by the finite difference analysis.

1. Introduction

A large and deep excavation in a soft soil area typically uses a support system consisting of a retaining wall with one or more levels of horizontal struts, which is costly and requires a long construction period [1]. Multibench retaining systems can be used to eliminate horizontal struts [2]. This retaining system has been used in several excavation projects in China [3, 4]. A typical two-bench retained excavation is shown in Figure 1. This retaining system consisted of two levels: double-row [5] and single-row [6, 7] contiguous pile walls were used as the first and second retaining structures, respectively.

Certain researches of multibench retaining system have been carried out in recent years. Zheng et al. [8] (2014) studied the stability and failure mechanism of the multibench retaining system using finite element method and material point method. Three failure modes of this retaining system were proposed based on the simulation results, that is, integrated failure, interactive failure, and disconnected failure. Further, Zheng et al. [2] designed and conducted a series of model tests to investigate the working and failure mechanism of the multibench retaining system and the three above-mentioned failure modes were also observed in these model tests.

Because the multibench retaining system does not have generally accepted design procedure and its geometry is similar to that of the earth berm supported wall/piles [9–14], the analysis method for earth berm [15] was usually applied in the design of the multibench retaining system in practice. However, this method neglects the restraint of the second retaining structure to the earth berm.

Bolton and Powrie [16] introduced the concept of "mobilizable soil strength (MSD)" to the design of cantilever retaining wall. Then, the MSD method was also applied to the prediction of the ground movements of braced excavations [17] and the design of the flexible walls propped at the crest [18]. Wang et al. [19] modified the MSD method by considering the undrained anisotropic shear strength of K_0 normally consolidated soft clay and bending strain energy of the retaining wall.

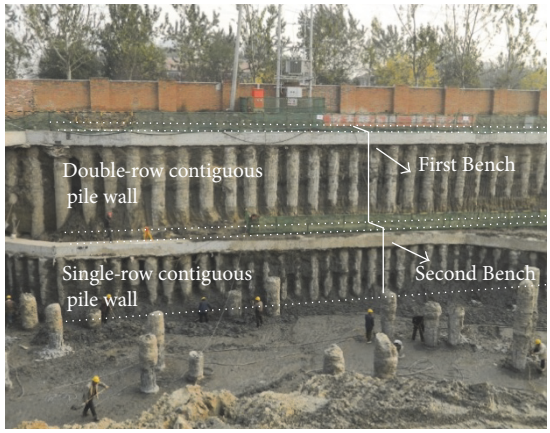

Figure 1: Photograph of a multibench retained excavation.

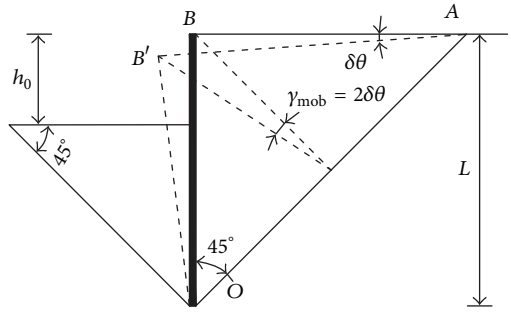

Figure 2: Kinematically admissible strain field of cantilever retaining wall in undrained condition [17].

Based on the MSD concept, a new design method for a two-bench retaining system considering the interaction of the first and second retaining structures is proposed in this paper. The results calculated using this method and those obtained by the finite difference method were well matched.

2. MSD Method for Cantilever Retaining Wall

Osman and Bolton [20] introduced the MSD design method for cantilever retaining wall. A kinematically admissible strain field of cantilever retaining wall in undrained condition was adopted in this method, as shown in Figure 2. In this strain field, the cantilever retaining wall rotates around a pivot point near the wall toe with a rotation angle of $\delta\theta$.

As the volumetric strain is 0 in undrained condition, the mobilized shear strain γ_{mob} is equal to $2\delta\theta$ [20].

Based on the stress-strain relation of the soil, the mobilized shear strength corresponding to γ_{mob} can be determined and will be referred to as c_{mob}. Osman and Bolton [20] proposed that the corresponding active and passive pressures mobilized at depth z can be given by

$$\begin{aligned} \sigma_a &= \gamma z + q_0 - 2c_{mob} \\ \sigma_p &= \gamma z + q_0 + 2c_{mob} \\ q_0 &= (K_0 - 1)(\gamma - \gamma_w) z, \end{aligned} \tag{1}$$

where σ_a and σ_b are the active and passive pressures, respectively; γ is the bulk unit weight of the soil; γ_w is the unit weight of water; q_0 is the initially mobilized deviator stress; and K_0 is the initial lateral earth pressure coefficient at rest.

The idealized stress distribution can be assumed as shown in Figure 3 [20]. z_c in Figure 3 is the depth of dry tension crack and can be calculated by

$$z_c = \frac{2c_{mob}}{\gamma + (K_0 - 1)(\gamma - \gamma_w)}. \tag{2}$$

If the wall height D, excavation height H, and bulk unit weight of soil are given, the mobilized shear strength c_{mob} and the height of the pivot point above the toe r can be determined by solving the equations of force and moment equilibrium. The stress-strain relationship at a representative point located at the middle height of the retaining wall is chosen to represent that in the entire admissible strain field [20]. Then, the corresponding γ_{mob} and $\delta\theta$ can be calculated.

3. MSD Method for Multibench Retained Excavation

For convenience, the first and second retaining structures are represented by 1RS and 2RS, respectively. The experimental results showed that the deformation mode of the retaining structures in multibench retained excavations was similar to that of the cantilever retaining structures (Zhang et al., 2016). The assumed strain field of cantilever retaining wall in undrained condition was accepted for each retaining structure in multibench retained excavation.

The strain field of multibench retaining system is shown in Figure 4. As the bench width (AB) is limited in multibench retaining system, the strain fields of the 1RS and 2RS are overlapped in the soil between two retaining structures (i.e., bench zone soil). As shown in Figure 4, the superimposed strain field is a pentagon, whose edges were AB, BC, CD, DE, and EA.

3.1. Shear Strain in Superimposed Strain Field. The core issue of MSD method for multibench retained excavation is the calculation of the shear strain in superimposed strain field. The superimposed strain field can be divided into three parts according to different mobilized shear strains, as shown in Figure 5.

For a soil element of part a in Figure 4, if the rotation angles of the 1RS and 2RS are $\delta\theta_1$ and $\delta\theta_2$, respectively, the horizontal displacements of the soil zone caused by the 1RS and 2RS are $h_1\delta\theta_1$ and $-h_2\delta\theta_2$ (the minus sign represents that the movement of the retaining structure tends to cause the soil zone to extend), respectively. h_1 and h_2 are the distance between the soil element and the toes of the 1RS and 2RS, respectively. The horizontal strain in part a $\delta\varepsilon_h^a$ can be calculated by

$$\delta\varepsilon_h^a = \frac{-h_2\delta\theta_2 + h_1\delta\theta_1}{B}, \tag{3}$$

where B is the length of the bench width (the length of AB in Figure 5).

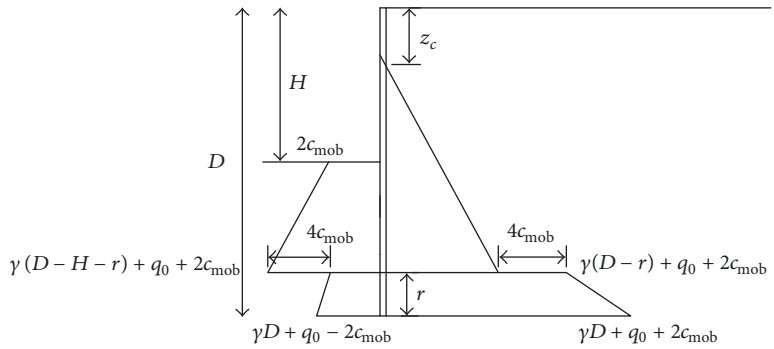

Figure 3: Lateral earth pressure distribution for an embedded cantilever wall in undrained conditions [20].

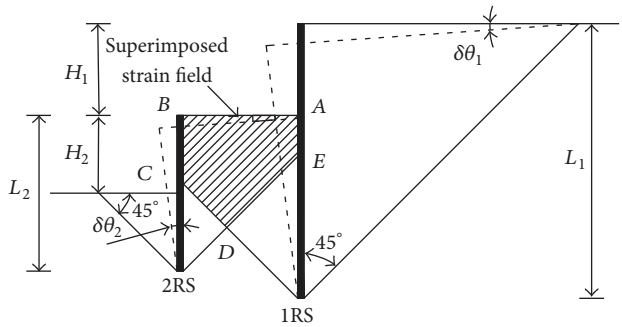

Figure 4: Kinematically admissible strain field of multibench retaining system.

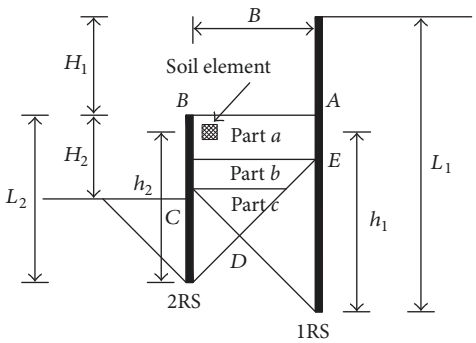

Figure 5: Different zones of the superimposed strain field for multibench retaining system.

Since the volume change is 0,

$$\delta\varepsilon_v^a = \delta\varepsilon_{\text{vol}}^a - \delta\varepsilon_h^a = \frac{h_2\delta\theta_2 - h_1\delta\theta_1}{B}, \tag{4}$$

where $\delta\varepsilon_v^a$ and $\delta\varepsilon_{vol}^a$ are the vertical and volume strain in part a.

The shear strain in part a $\delta\varepsilon_s^a$ is given by

$$\delta\varepsilon_s^a = \delta\varepsilon_v^a - \delta\varepsilon_h^a = \frac{2h_2\delta\theta_2 - 2h_1\delta\theta_1}{B}. \tag{5}$$

For a soil zone in part b, the horizontal strain in part b $\delta\varepsilon_h^b$ can be calculated by

$$\delta\varepsilon_h^b = \frac{-h_2\delta\theta_2}{h_2} + \frac{h_1\delta\theta_1}{B} = -\delta\theta_2 + \frac{h_1\delta\theta_1}{B}. \tag{6}$$

The vertical strain $\delta\varepsilon_v^b$ and shear strain $\delta\varepsilon_s^b$ in part b can be given by

$$\delta\varepsilon_v^b = \delta\varepsilon_{\text{vol}}^b - \delta\varepsilon_h^b = \delta\theta_2 - \frac{h_1\delta\theta_1}{B}, \tag{7}$$

$$\delta\varepsilon_s^b = \delta\varepsilon_v^b - \delta\varepsilon_h^b = 2\delta\theta_2 - \frac{2h_1\delta\theta_1}{B}, \tag{8}$$

where $\delta\varepsilon_{\text{vol}}^b$ is the volume strain in part b.

For a soil zone in part c, the horizontal strain in part c $\delta\varepsilon_h^c$ can be calculated by

$$\delta\varepsilon_h^c = \frac{-h_2\delta\theta_2}{h_2} + \frac{h_1\delta\theta_1}{h_1} = -\delta\theta_2 + \delta\theta_1. \tag{9}$$

The vertical strain $\delta\varepsilon_v^c$ and shear strain $\delta\varepsilon_s^c$ in part c can be given by

$$\delta\varepsilon_v^c = \delta\varepsilon_{\text{vol}}^c - \delta\varepsilon_h^c = \delta\theta_2 - \delta\theta_1 \tag{10}$$

$$\delta\varepsilon_s^c = \delta\varepsilon_v^c - \delta\varepsilon_h^c = 2\delta\theta_2 - 2\delta\theta_1, \tag{11}$$

where $\delta\varepsilon_{\text{vol}}^c$ is the volume strain in part c.

In (5), (8), and (11), the superimposed shear strains are related to the bench width and the distances between the soil zone and the toes of the 1RS and 2RS. For different geometry of multibench retaining system, the superimposed strain field and its shear strains are variable. As shown in Figure 6, there are 5 different superimposed strain fields (including that shown in Figure 4) according to the different interfaces of the superimposed strain fields and retaining

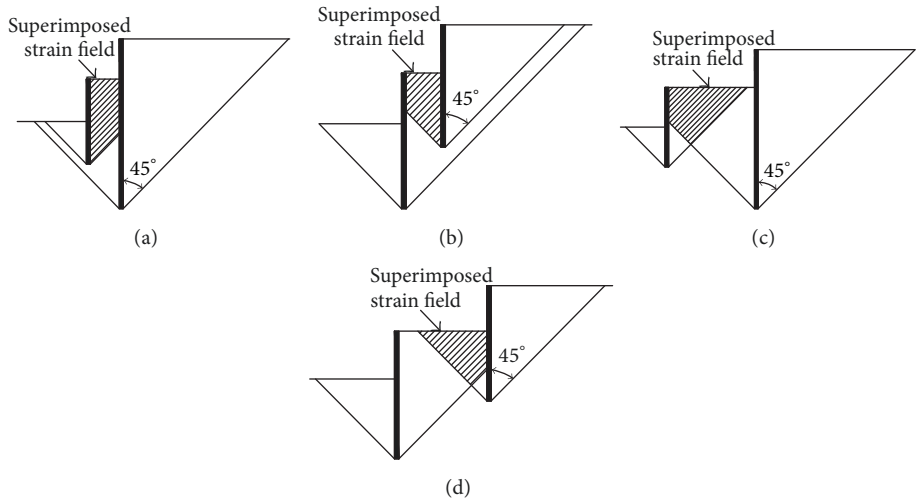

Figure 6: Different contact relations of the superimposed strain fields and retaining structures.

structures. The weighted average superimposed shear strain $\delta\varepsilon_s^d$ is adopted to represent the mobilized shear strain in the entire superimposed strain field to simplify the analysis procedure. The superimposed shear strain can be calculated by

$$\delta\varepsilon_s^d = \frac{A_a\delta\varepsilon_s^a + A_b\delta\varepsilon_s^b + A_c\delta\varepsilon_s^c}{A_a + A_b + A_c}, \tag{12}$$

where A_a, A_b, and A_c are the areas of parts a, b, and c in the superimposed strain field, respectively. $A_a\delta\varepsilon_s^a$, $A_b\delta\varepsilon_s^b$, and $A_c\delta\varepsilon_s^c$ can be calculated through the integral along h_1 and h_2. According to the stress-strain relation of the soil, $\delta\theta_1$ and $\delta\theta_2$ can be expressed by the mobilized shear strength of the 1RS c_{m1} and that of the 2RS c_{m2}, which is

$$\delta\varepsilon_s^d = f\left(c_{m1}, c_{m2}\right). \tag{13}$$

3.2. Earth Pressures Acting on 1RP and 2RP. In the multi-bench retaining system, the earth pressure exerted on the retaining structures by the soil in the normal strain field is equal to that of cantilever retaining wall, whereas the earth pressure exerted by the soil in the superimposed strain field is determined by the weighted average superimposed shear strain. Taking the pattern in Figure 4 as an example, because the embedded ratio of 2RP is smaller than that of 1RP, $\delta\theta_2$ may be larger than $\delta\theta_1$. Therefore, assume that $\delta\varepsilon_s^d$ is negative, and then the lateral earth pressure distribution acting on the 1RS can be illustrated as that in Figure 7.

In Figure 7, z_1 is the depth of dry tension crack for the 1RS and can be calculated by

$$z_1 = \frac{2c_{m1}}{\gamma - (1 - K_0)(\gamma - \gamma_w)}. \tag{14}$$

The earth pressures in the active side of the 1RS in Figure 7 are given by

$$s_{11a} = \gamma_w(L_1 - R_1) + K_0(\gamma - \gamma_w)(L_1 - R_1) - 2c_{m1}$$

$$s_{11p} = \gamma_w(L_1 - R_1) + K_0(\gamma - \gamma_w)(L_1 - R_1) + 2c_{m1}$$

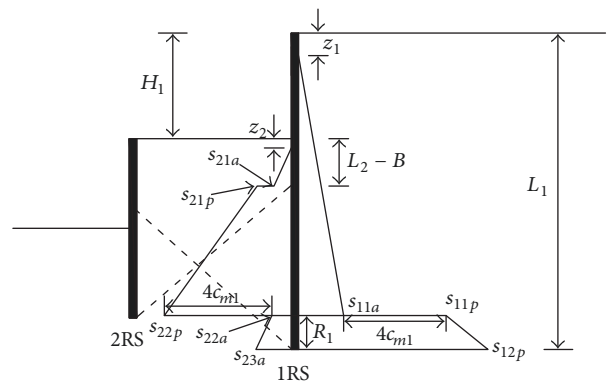

Figure 7: Lateral earth pressure distribution for the 1RS.

$$s_{12p} = \gamma_w L_1 + K_0(\gamma - \gamma_w) L_1 + 2c_{m1}, \tag{15}$$

where L_1 is the length of the 1RS and R_1 is the height of the pivot point above the toe of the 1RS.

For the passive side of the 1RS, as $\delta\varepsilon_s^d$ is assumed to be negative, which means that the soil in the superimposed strain field tends to be extended, the earth pressure exerted by the soil in the superimposed strain field tends to an active state and dry tension crack will form in the passive side of 1RP, as shown in Figure 7. If the stress-strain relationship for the representative point of the 1RS can be expressed by $\delta\varepsilon_{s1} = f_1(c_{m1})$, the tension crack depth and the earth pressure acting on the passive side can be given by

$$z_2 = \frac{\left|2f_1^{-1}\left[f\left(c_{m1}, c_{m2}\right)\right]\right|}{\gamma - (1 - K_0)(\gamma - \gamma_w)}$$

$$s_{21a} = \gamma_w(L_2 - B) + K_0(\gamma - \gamma_w)(L_2 - B) - \left|2f_1^{-1}\left[f\left(c_{m1}, c_{m2}\right)\right]\right|$$

$$s_{21p} = \gamma_w(L_2 - B) + K_0(\gamma - \gamma_w)(L_2 - B) + 2c_{m1}$$

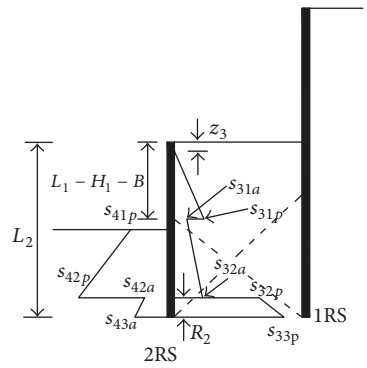

FIGURE 8: Lateral earth pressure distribution for 2RS.

$$\begin{aligned}
s_{22p} &= \gamma_w (L_1 - H_1 - R_1) \\
&\quad + K_0 (\gamma - \gamma_w)(L_1 - H_1 - R_1) + 2c_{m1} \\
s_{22a} &= \gamma_w (L_1 - H_1 - R_1) \\
&\quad + K_0 (\gamma - \gamma_w)(L_1 - H_1 - R_1) - 2c_{m1} \\
s_{23a} &= \gamma_w (L_1 - H_1) + K_0 (\gamma - \gamma_w)(L_1 - H_1) - 2c_{m1},
\end{aligned} \tag{16}$$

where z_2 is the dry tension crack formed in the passive side of the 1RS, L_2 is the length of the 2RS, and H_1 is the height of the first excavation.

The lateral earth pressure distribution acting on the 2RS can be illustrated as that in Figure 8. The tension crack depth and the earth pressures acting on the active side of the 2RS can be given by

$$\begin{aligned}
z_3 = z_2 &= \frac{\left|2 f_2^{-1}\left[f(c_{m1}, c_{m2})\right]\right|}{\gamma - (1 - K_0)(\gamma - \gamma_w)} \\
s_{31p} &= \gamma_w (L_1 - H_1 - B) + K_0 (\gamma - \gamma_w)(L_1 - H_1 - B) \\
&\quad - \left|2 f_2^{-1}\left[f(c_{m1}, c_{m2})\right]\right| \\
s_{31a} &= \gamma_w (L_1 - H_1 - B) + K_0 (\gamma - \gamma_w)(L_1 - H_1 - B) \\
&\quad - 2c_{m2} \\
s_{32a} &= \gamma_w (L_2 - R_2) + K_0 (\gamma - \gamma_w)(L_2 - R_2) - 2c_{m2} \\
s_{32p} &= \gamma_w (L_2 - R_2) + K_0 (\gamma - \gamma_w)(L_2 - R_2) + 2c_{m2} \\
s_{33p} &= \gamma_w L_2 + K_0 (\gamma - \gamma_w) L_2 + 2c_{m2},
\end{aligned} \tag{17}$$

where z_3 is the dry tension crack formed in the active side of the 2RS, R_2 is the height of the pivot point above the toe of the 2RS, and $\delta\varepsilon_2 = f_2(c_{m2})$ is the stress-strain relationship for the representative point of the 2RS. As the lengths and embedded situations of the 1RS and 2RS are different, the representative points and their stress-strain relationships are different.

The earth pressures acting on the passive side of the 2RS can be given by

$$\begin{aligned}
s_{41p} &= 2c_{m2} \\
s_{42p} &= \gamma_w (L_2 - H_2 - R_2) \\
&\quad + K_0 (\gamma - \gamma_w)(L_2 - H_2 - R_2) + 2c_{m2} \\
s_{42a} &= \gamma_w (L_2 - H_2 - R_2) \\
&\quad + K_0 (\gamma - \gamma_w)(L_2 - H_2 - R_2) - 2c_{m2} \\
s_{43a} &= \gamma_w (L_2 - H_2) + K_0 (\gamma - \gamma_w)(L_2 - H_2) - 2c_{m2},
\end{aligned} \tag{18}$$

where H_2 is the depth of the second excavation.

3.3. MSD Analysis Procedure. In (14)–(18), there are 4 unknown parameters, which are c_{m1}, c_{m2}, R_1, and R_2. Meanwhile, there are 2 force equilibrium equations and 2 moment equilibrium equations for the 1RS and 2RS. Therefore, the unknown parameters can be solved.

The analysis procedures of the multibench retaining system using MSD method can be summarized as follows.

(1) Select the representative points of stress-strain relation for the 1RS and 2RS, respectively.

(2) Calculate the weighted average superimposed shear strain $\delta\varepsilon_s^d$.

(3) Determine the relationship between $\delta\varepsilon_s^d$ and c_{m1}, c_{m2}, according to the representative stress-strain relationship of the 1RS and 2RS.

(4) Determine the earth pressure distribution modes acting on the 1RS and 2RS based on the geometry of the superimposed strain field.

(5) Calculate c_{m1}, c_{m2}, R_1, and R_2 by solving the equations of force and moment equilibrium of the 1RS and 2RS.

(6) Calculate the mobilized shear strains of the 1RS and 2RS. Then, the crest displacements of the 1RS and 2RS can be calculated based on $\delta\theta_1$ and $\delta\theta_2$.

4. Finite Difference (FD) Analysis

To verify the accuracy of the MSD method for multibench retaining system, a two-dimensional plane strain finite difference analysis was performed to predict the behavior of a two-bench retained excavation. Half of the excavation was modeled and the finite difference model is shown in Figure 9. The first and second excavation depths (H_1 and H_2) were both 4 m. The bench width B was 8 m. The retaining structures were assumed to be 1 m thick retaining walls. The lengths of the 1RS and 2RS, L_1 and L_2, were 24 m and 12 m, respectively. The left and right boundaries of the numerical model were fixed with roller supports, and the bottom boundary was fixed with pin supports.

As Speswhite China kaolin was widely used in geotechnical research and its properties were well known; the soil layer was modeled using Speswhite China kaolin [21]. The soil

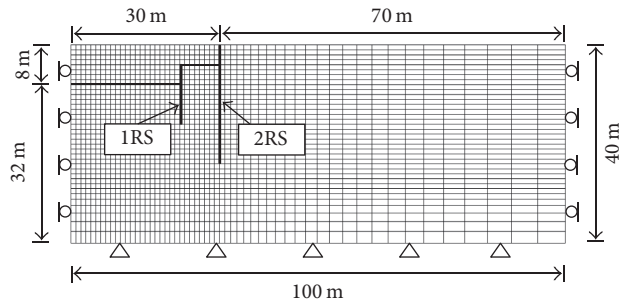

Figure 9: Finite difference mesh.

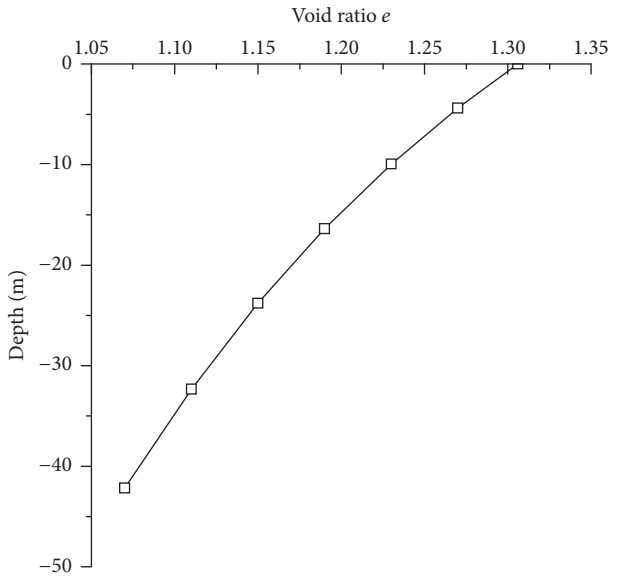

Figure 10: Void ratio of the overconsolidated soil.

Table 1: Material parameters of kaolin clay [23].

Parameter	Value
Bulk weight (kN/m^3)	17.6
Stress ratio, M	0.84
Slope of one-dimensional compression line in v–lnp' space, λ	0.25
Slope of unload–reload line in v–lnp' space, κ	0.05
Specific volume of the critical state line at unit pressure, Γ	3.48
Poisson's ratio for effective stress analysis, ν'	0.33
Coefficient of earth pressure at rest, K_0	0.63
Saturated horizontal permeability, k_h (m/s)	4.43×10^{-9}
Saturated vertical permeability, k_v (m/s)	2.89×10^{-9}

was overconsolidated by applying 200 kPa vertical loading on top of the soil surface. According to critical state soil mechanics [22], the void ratio of the overconsolidated soil can be calculated, as shown in Figure 10.

The Modified Cam-clay (MCC) model was adopted to simulate the soil. The material parameters of kaolin clay are shown in Table 1.

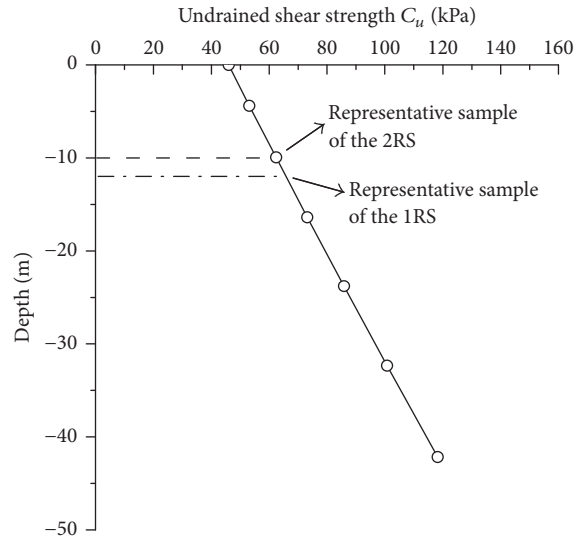

Figure 11: Undrained strength profile.

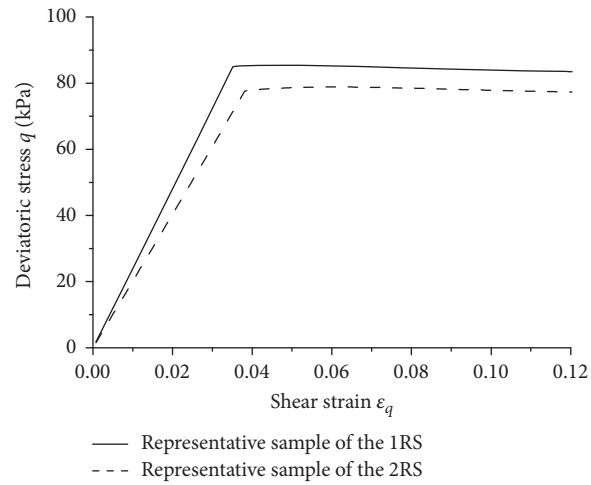

Figure 12: Representative stress (q)-strain (ε_q) curve for the 1RS and 2RS.

The retaining structures were made of reinforced concrete and simulated by liner elements, which have interfaces on both sides. The retaining structures were assumed to be elastic. Young's modulus and the equivalent thickness of the liner were determined to be 30 GPa and 1 m. The friction angle of the interface of the soil and retaining structures was 16.7°.

Water table was located at the ground surface. As the excavation process was assumed to be conducted in a very short period, undrained condition was applied and the seepage flow was not allowed during the excavation.

5. Comparison between MSD and FD

The undrained shear strength in MCC model can be calculated and is shown in Figure 11. The representative point was located at the middle height of each retaining structure. The representative stress (q)-strain (ε_q) curve is shown in Figure 12.

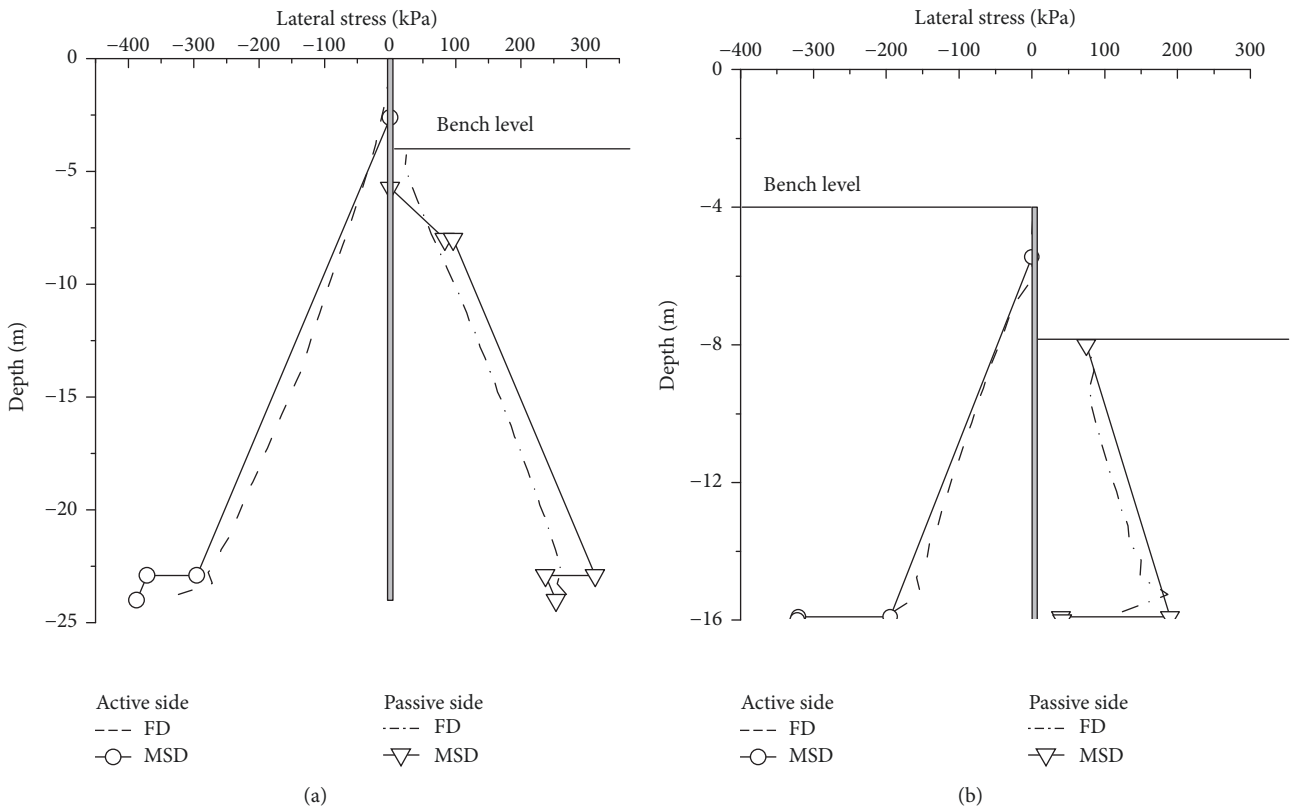

Figure 13: Lateral stress distribution: (a) 1RS and (b) 2RS.

Table 2: The displacements calculated by the MSD and FD method.

	c_{m1} or c_{m1} (kPa)	R_1 or R_2 (m)	Crest displacement (MSD) (cm)	Crest displacement (FD) (cm)
1RS	19.0	1.1	29.94	27.56
2RS	37.4	0.1	25.63	32.75

According to (5), (8), (11), and (12), the weighted average superimposed shear strain can be given by $\delta\varepsilon_s^d = (9/4)\delta\theta_2 - (47/12)\delta\theta_1$. The calculated result of the mobilized shear strength of the 1RS c_{m1} is 19 kPa and R_1 is 1.1 m. The mobilized deviatoric stress is given by $q_{m1} = 2c_{m1} = 38$ kPa. From the stress-strain curve, the corresponding triaxial shear strain ε_{q1} is 0.0159. The engineering shear strain ε_{s1} is equal to 1.5 times the triaxial shear strain ε_{q1} [20], and thus $\varepsilon_{s1} = 1.5\varepsilon_{q1} = 0.02385$. The rotation angle of the 1RS is given by $\delta\theta_1 = \varepsilon_{s1}/2 = 0.01193$. The height of the wall above the pivot point is calculated by $L_1' = L_1 - R_1 = 23.1$ m. Thus, the crest horizontal displacement of the 1RS is $L_1'\delta\theta_1 = 27.56$ cm. The crest displacement of the 2RS can be calculated through the same procedure above.

The results predicted by the MSD and FD method are listed in Table 2. The calculated crest displacements of the 1RS and 2RS using the MSD method were close to those calculated using the FD analysis.

Figure 13 shows the lateral earth pressures acting on the 1RS and 2RS predicted by the MSD and FD method. The predicted results are close to each other.

The bending moment distributions of the 1RS and 2RS are shown in Figure 14. As the retaining structures were assumed to be rigid, the MSD calculated results are larger than the FD results. When the retaining structures are more rigid, the FD results will be closer to the MSD results, as shown in Figure 14.

Osman and Bolton [20] discussed the influence of flexibility of the retaining wall. If a ductile retaining structure is designed to resist MSD earth pressure, it would attract smaller moment than the calculated value and cannot collapse, which is on the safe side. If it is so stiff that it would develop bending moments in excess of the MSD values, extra plastic displacements would be caused to relieve the earth pressures and reduce the bending moments [20].

6. Conclusions

The analysis method for the multibench retaining system based on the MSD theory was introduced in this paper. The kinematically admissible deformation mechanism of cantilever retaining wall is adopted to represent the deformation characteristics of the 1RS and 2RS in a two-bench retaining system. The weighted average shear strain of the superimposed strain field and the lateral earth pressure distributions acting on each retaining structure were deduced

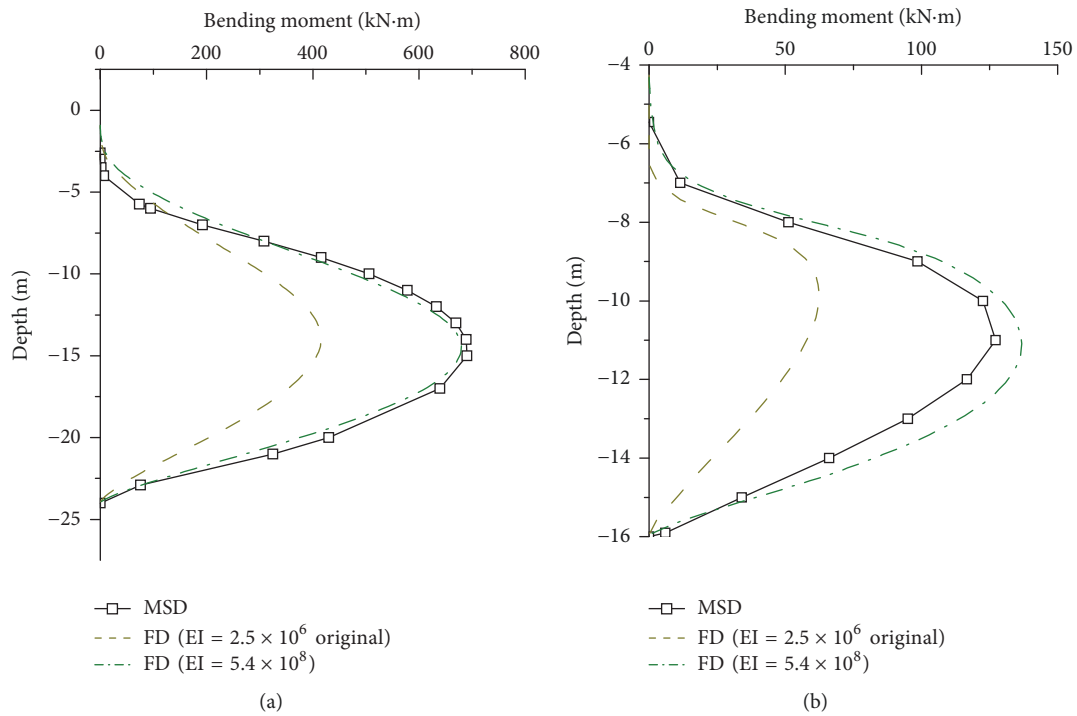

Figure 14: Bending moment distribution: (a) 1RS and (b) 2RS.

based on the MSD concept. Following the MSD analysis procedure proposed in this paper, the crest displacements, earth pressures, and bending moment in a two-bench retained excavation can be calculated using this method. Basically, the MSD calculated results matched the finite difference results.

Conflicts of Interest

The authors declare that they have no conflicts of interest.

Acknowledgments

This work was supported by the National Natural Science Foundation of China (Grants nos. 51508382 and 41630641) and the National Key Research and Development Program of China (Grant no. 2017YFC0805407). Their support is gratefully acknowledged.

References

[1] M.-L. Yang, S.-J. Chen, and S.-T. Chen, "Innovative central opening strut system for foundation excavation," *Journal of Construction Engineering and Management*, vol. 132, no. 1, pp. 58–66, 2006.

[2] G. Zheng, D. Q. Nie, Y. Diao et al., "Numerical and Experimental Study of Multi-Bench Retained Excavations," *Geomechanics and Engineering*, 2017.

[3] Q. P. Weng and W. D. Wang, "Design and construction of multilevel supporting system for deep foundation pits excavation of Shanghai Hongqiao Integrated Transport Hub," *Bu. Str*, vol. 45, no. 5, pp. 172–176, 2012.

[4] G. Zheng, Y. Du, X. Cheng, Y. Diao, X. Deng, and F. Wang, "Characteristics and prediction methods for tunnel deformations induced by excavations," *Geomechanics and Engineering*, vol. 12, no. 3, pp. 361–397, 2017.

[5] C.-J. Lee, Y.-C. Wei, H.-T. Chen, Y.-Y. Chang, Y.-C. Lin, and W.-S. Huang, "Stability analysis of cantilever double soldier-piled walls in sandy soil," *Journal of the Chinese Institute of Engineers, Transactions of the Chinese Institute of Engineers,Series A/Chung-kuo Kung Ch'eng Hsuch K'an*, vol. 34, no. 4, pp. 449–465, 2011.

[6] M. D. Bolton and W. Powrie, "The collapse of diaphragm walls retaining clay," *Géotechnique*, vol. 37, no. 3, pp. 335–353, 1987.

[7] A. Ouria, V. Toufigh, C. Desai, V. Toufigh, and H. Saadatmanesh, "Finite element analysis of a CFRP reinforced retaining wall," *Geomechanics and Engineering*, vol. 10, no. 6, pp. 757–774, 2016.

[8] G. Zheng, X. Cheng, and Y. Diao, "Analysis of the stability and collapse mechanism of non-prop and multi-stage retaining structure," *Journal of Tianjin University (Science and Technology)*, vol. 46, no. 4, pp. 304–314, 2013.

[9] M. P. Daly and W. Powrie, "Undrained analysis of earth berms as temporary supports for embedded retaining walls," *Journal of Geotechnical Engineering*, vol. 149, no. 4, pp. 237–248, 2001.

[10] G. W. Clough and R. R. Davidson, "Effects of construction on geotechnical performance," in *Proceedings of the Ninth International Conference Soil Mechanics and Foundation Engineering, Specialty Session III*, pp. 15–53, 1977.

[11] M. Georgiadis and C. Anagnostopoulos, "Effect of berms on sheet-pile wall behaviour," *Géotechnique*, vol. 48, no. 4, pp. 569–574, 1998.

[12] S. M. Gourvenec and W. Powrie, "Three-dimensional finite element analyses of embedded retaining walls supported by

discontinuous earth berms," *Canadian Geotechnical Journal*, vol. 37, no. 5, pp. 1062–1077, 2000.

[13] D. M. Potts, T. I. Addenbrooke, and R. A. Day, "The use of soil berms for temporary support of retaining walls," *Retaining structures. Proc. conference, Cambridge, 1992*, pp. 440–447, 1993.

[14] W. Powrie and M. P. Daly, "Centrifuge model tests on embedded retaining walls supported by earth berms," *Géotechnique*, vol. 52, no. 2, pp. 89–106, 2002.

[15] M. P. Daly and W. Powrie, "Undrained analysis of earth berms as temporary supports for embedded retaining walls," *Proceedings of the Institution of Civil Engineers: Geotechnical Engineering*, vol. 149, no. 4, pp. 237–248, 2001.

[16] M. D. Bolton and W. Powrie, "Behaviour of diaphragm walls in clay prior to collapse," *Géotechnique*, vol. 38, no. 2, pp. 167–189, 1988.

[17] A. S. Osman and M. D. Bolton, "Ground movement predictions for braced excavations in undrained clay," *Journal of Geotechnical and Geoenvironmental Engineering*, vol. 132, no. 4, pp. 465–477, 2006.

[18] M. Diakoumi and W. Powrie, "Mobilisable strength design for flexible embedded retaining walls," *Géotechnique*, vol. 63, no. 2, pp. 75–106, 2013.

[19] H. Wang, W. Wang, M. Huang, and Z. Xu, "Modified mobilizable strength design (MSD) method on deformation predictions of foundation pit," *Chinese Journal of Rock Mechanics and Engineering*, vol. 30, no. 1, pp. 3245–3251, 2011.

[20] A. S. Osman and M. D. Bolton, "A new design method for retaining walls in clay," *Canadian Geotechnical Journal*, vol. 41, no. 3, pp. 451–466, 2004.

[21] A. Ardakani, M. Bayat, and M. Javanmard, "Numerical modeling of soil nail walls considering Mohr Coulomb, hardening soil and hardening soil with small-strain stiffness effect models," *Geomechanics and Engineering*, vol. 6, no. 4, pp. 391–401, 2014.

[22] D. M. Wood, *Soil Behaviour and Critical State Soil Mechanics*, Cambridge University Press, Cambridge, 1991.

[23] Y. Hong and C. W. W. Ng, "Base stability of multi-propped excavations in soft clay subjected to hydraulic uplift," *Canadian Geotechnical Journal*, vol. 50, no. 2, pp. 153–164, 2013.